Genetic Optimization of Edge Treatments of Single Offset Reflector Compact Antenna Test Ranges

M. Dirix[1]
[1]Antenna Systems Solutions
Isabel Torres 9,
39011 Santander, Spain,
mdirix@asysol.com

S.F. Gregson[2, 3]
[2]Next Phase Measurements
11521 Monarch St, Garden Grove,
CA, USA

R.R. Dubrovka[3]
[3]Queen Mary University of London,
School of Electronic Engineering
and Computer Science
London, UK,

***Abstract*—This paper presents the results of a continuation of the authors prior study into the optimization of compact antenna test ranges (CATR) using evolutionary algorithms. The authors existing algorithm was improved and extended to provide broadband optimization of serrated edge and blended rolled edge (BRE) CATRs before using this refined algorithm to, for the first time, take account of chamber wall illumination in the case of blended rolled edge CATRs which is a recognized deficiency of this approach. This paper presents performance predictions of CATRs that, in addition to being optimized for quiet-zone performance, are also optimized to reduce chamber wall illumination. Performance predictions of example CATR designs are presented, compared and contrasted.**

***Index Terms*—CATR, Evolutionary Computing, Edge Treatment, Serrated Edge, Blended Rolled Edge, Quiet Zone, Chamber Optimization.**

I. Introduction

Direct far-field testing has become the baseline test methodology for sub-6 GHz over the air (OTA) testing of the physical layer of radio access networks [1]. However, the proliferation of mm-wave massive multiple input multiple output (Massive MIMO) antennas for 5G New Radio rollout and the use of complex waveforms for communication system testing and primary Figure of Merit determination has necessitated the adoption of the Compact Antenna Test Range (CATR) as the preferred test solution [2]. The CATR was initially conceived as comprising an efficient way of testing electrically large antennas at very much reduced, fixed, range lengths [3]. However, early workers quickly recognized that the reflector edge treatment, feed spillover, and chamber wall illumination are significant factors determining the quality and purity of the collimated pseudo plane-wave with this becoming especially important at mm-wave frequencies [3]. Using modern powerful, parallelized, digital computational simulation techniques in combination with broadband genetic optimization [4, 5], the edge treatment can be evolved for a specific CATR application as part of the design process for a range of reflector edge treatments [6, 7, 8]. This paper extends the authors previous work to include more sophisticated reflector edge treatments than have hitherto been considered within the design and broadband genetic optimization procedure, while also taking into account wall illumination. The next section concentrates upon refining and improving the performance of the genetic optimization algorithm before harnessing this approach for the design and optimization of a blended rolled edge CATR which, for the first time, takes in account chamber wall illumination.

II. Broadband Genetic Optimization

The inherent broadband nature of CATRs can perhaps be best seen to stem from the geometrical optics basis of their principle of operation [8]. Although this could suggest that their design is automatically broadband in nature, which for the most part it is, it is also well known that amplitude and phase ripple are largely governed by edge diffraction effects, which are phenomena that are most certainly frequency dependent [8]. The problems associated with reflector edge diffraction were quickly identified as constituting a critical issue in the successful implementation of CATRs. Therefore, an extensive investigation of the applicable bandwidth of a single-frequency optimized CATR solution is important. In this section, the frequency dependent behaviour of a single frequency optimized CATR design is examined. Crucially, the results obtained provide a strong indication as how best to choose the optimization strategy.

A rectangular blended rolled edge (BRE) [8, 9] CATR was optimized using the simulation technique developed in [4, 8], and the genetic optimization (GO) strategy presented previously within [9, 10], and using the CATR geometry detailed in [10]. The GO was performed at 8.2, 10.0, 12.4, 18.0, 26.0 and 40.0 GHz, using consistent optimization parameters. A population of one hundred reflector profiles were initially generated at random that spanned the design space whose domain was bounded by predefined geometrical constraints. The "best" six parents were taken and used to breed a new generation of twenty-four parameter (gene) mixed and permuted children [9, 10]. This process was repeated until the termination requirement was satisfied, which was based on either minimal variation of the penalty function, or maximum runtime of 400 generations. It is noted here, that depending on frequency; between 40 and 340 generations were required for the optimization process to converge and complete. This point will be further discussed later in this section (*cf*. Fig 2).

Once the optimisation was completed, the CATR quiet-zone (QZ) was computed whereupon all of the standard CATR performance metrics were derived [8]. This can be seen illustrated in Fig. 1 which shows the maximum amplitude- and phase-variations plotted as a function of operational frequency where each trace represents the performance of a CATR solution found after optimization at a *different* optimization frequency. It is perhaps worth emphasizing here that this

exhaustive simulation study comprised the computation of *circa* 100,000 individual CATRs and their respective QZ performance metrics *per* feed tilt angle. Such an exhaustive study was only made possible through the efficiency of the parallelised implementation of the field propagation algorithm [6, 7, 8].

From the results presented in Fig. 1, it is clear that the performance improvement achieved while optimizing at lower frequencies remain when the range is used at higher frequencies. This is a crucial observation. It is further worth noting that the optimization performed at too low frequencies (*e.g.* reflector size of less than *circa* 20 wavelengths across) gives potentially less reliable designs with behaviour that is more variable with increasing frequency. Note that this was more prominent when inspecting the total phase variation.

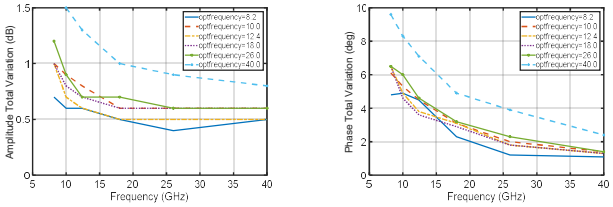

(a) (b)

Fig. 1. Total amplitude (a) and phase (b) variation over frequency for 27 (deg) feed offset angle.

However, the present results clearly illustrate that optimization at higher frequencies require some additional tuning of the optimizer, with especially the exit strategy needing to be adapted. As noted above, this is a consequence of the QZ ripple becoming less sensitive to subtle changes within the reflector edge as the electrical size of the reflector increases. This resulted in a corresponding reduction in the variation of the penalty function from generation to generation which, leads in turn to the increased likelihood that the optimizer could settle at a local minimum of the penalty function. This can also be concluded from Fig. 2, where a higher frequency optimization leads to a reduction in the number of iterations of the optimizer. Here, Fig. 2 presents a plot of the number of generations required at each optimization frequency for the 27° feed offset angle, as well as for several other feed angles which all show the same trend when allowing for the stochastic nature of the optimization process, *cf.* 10 GHz 27° feed tilt angle case. It can thus be concluded that the convergence is optimization-frequency dependent, having a more rapid convergence at a higher optimization frequency. This is again expected to be caused due to the stronger impact of the edge treatment at lower frequencies on the QZ ripple behaviour, and thus variation of the penalty function, on which the exit criteria is based, leading to the optimizer settling at a local minimum of the penalty function.

As anticipated, with the refined exit strategy employing a tougher criterion we could see an increased number of iterations being required before converging on the final result, with the resulting QZ performance and reflector design being very comparable with the previous optimizations that were derived at lower optimisation frequencies. This can be seen illustrated in Fig. 3 which present the total amplitude (a), and phase (b), variation over frequency for 27° feed offset angle for the 40 GHz optimisation frequency "before" and "after" refinement of the GO exit strategy, as denoted by the blue and red traces respectively. Additionally, a measure of how "hard" the GO is having to work can be obtained from noting the number of generations required to breed an optimum solution, as well as the variance of the of the penalty function inside the population which also stabilised across optimisation frequency.

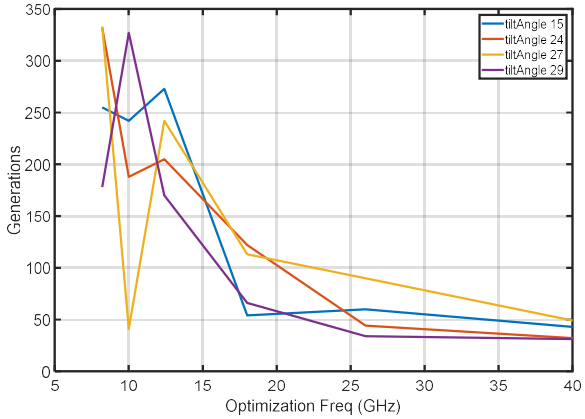

Fig. 2. Number of generations required versus optimization frequency.

This particular effect was mostly dominant in the highest optimization frequency of 40 GHz. In order to investigate the effect in more detail, the exit strategy was further optimized based on the expected variation of the penalty function.

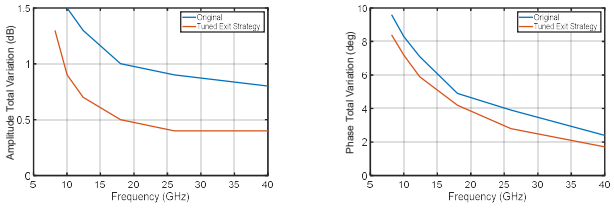

(a) (b)

Fig. 3. Total amplitude (a) and phase (b) variation over frequency for 27 (deg) feed offset angle, before (blue) and after (red) refining the GO exit strategy.

Additionally, Fig. 4 presents comparisons of the BRE CATR reflector optimized shapes for the cases where the optimization was run respectively at 10 GHz, 40 GHz before refinement, and 40 GHz after refinement. Here it is clear that with the GO adaption that we are able to obtain reflector surfaces that are very similar in form, with more minor variation resulting from the specific application frequency band being considered. This serves as further confirmation of the success of the approach.

(a) (b) (c)

Fig. 4. Comparison of BRE Reflector shapes (*not* drawn to scale) at 10 GHz (a), 40 GHz (b) and 40 GHz (c) with refined exit strategy.

III. Relationship Between Reflector Edge Treatment and Chamber Wall Illumination

There are several methods of minimising reflector edge diffraction effects [8]. The concept of the serrated edge is that the continually changing edge angle spreads the diffracted energy over a wider region in the quiet zone and so avoids constructive mixing of the individual diffraction points that is seen on a simple straight or curved knife edge to the reflector. In contrast, and as can be seen in Fig. 5, the blended rolled edge (BRE) reflector uses a smooth transition from the parabolic reflector surface that collimates the feed quasi spherical wave to the quiet zone, to an elliptic surface that progressively steers the energy away from the quiet zone. These respective approached have a range of merits including cost and complexity however here, we shall primarily restrict ourselves to consider the diffraction effects. A comparison of the ray paths resulting from the focal point feed illumination of a parabola for both serrations and blended rolled edge treatment can be seen illustrated in Fig. 5, which is a reproduction of Figure 5.21 of [8].

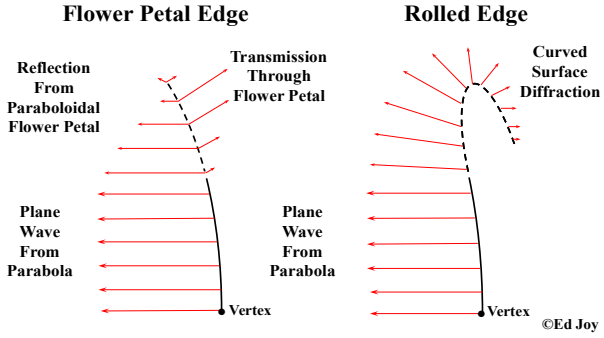

Fig. 5. Ray paths resulting from focal point feed illumination of a parabola for both serrations and blended rolled edge treatment, reproduction of Figure 5.21 of [8], courtesy of Ed Joy.

With this in mind, let us evaluate the QZ and chamber illumination for comparable serrated edge (SE) and BRE edge CATRs for a given fixed geometry, feed, and frequency. Fig. 6 shows the examples of a SE and equivalent BRE CATR that are conceived for testing at mm-wave frequencies in a 5GNR Over the Air application.

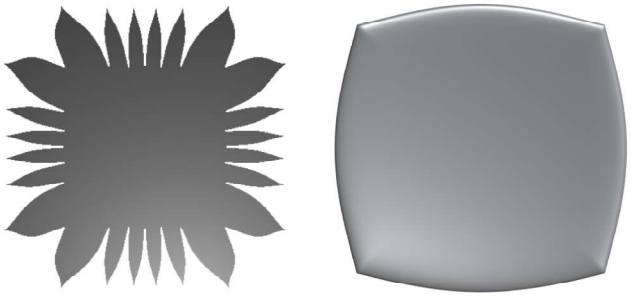

(a) (b)

Fig. 6. Serrated edge (a) and, blended rolled edge (b) reflector CATRs.

Here, the parabolic solid regions of the reflectors were consistent, as was the maximum external dimensions; with the edge treatment occupying equivalent projected areas and both comprise virtual vertex CATR designs. Fig. 7 shows the fields reflected from the respective CATR reflectors at 26 GHz that illuminate the walls of an enclosing chamber that is 1.5 × 1.5 × 3 m [H × W × L]. The feed illumination is consistent between the respective configurations and as such is auxiliary to this particular comparison. As is commonplace, in each of these examples, the CATR is corner fed with the circular horn feed being tilted so that the boresight direction is orientated to point just beyond the geometrical center of the reflector so as to best equalize the amplitude taper within the CATR QZ.

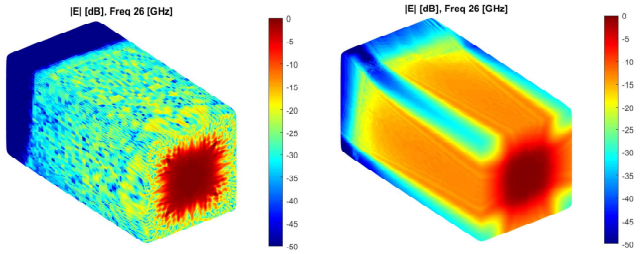

(a) (b)

Fig. 7. Comparison of CATR fields reflected from SE (a) and, BRE (b) reflectors at 26 GHz.

Here, the wall illuminations are computed from the field reflected by the CATR reflector using the current element method [4, 8], *i.e.* the direct feed illumination is not included here [8]. This clearly illustrates where the largest field intensities are located on the chamber walls, and can be used to aid in the design of the chamber absorber layout and the reflector edge treatment itself. Furthermore, it also confirms that for the case of the serrated edge reflector the collimated pseudo-plane wave mostly illuminates the wall behind the AUT at largely normal incidence, which is the direction in which the, typically, pyramidal absorber performs the best. In contrast, the blended rolled edge CATR illuminates much of the chamber walls with comparatively large amounts of field, including the spectral directions, and it does so over a *wide* range of incidence angles, even approaching grazing angles where the performance of typical absorber degrades noticeably. For example a piece of, say, pyramidal absorber that is 4 wavelengths thick provides absorption of *circa* 50 dB at normal incidence, *i.e.* at 0°. However, there is a significant reduction in absorption when being illuminated from non-incidence angles. For example, at 60° away from normal the absorption will have reduced to *circa* 38 dB, at 70° this will be *circa* 30 dB ,and at 80°, *i.e.* at grazing angles, it will be further reduced to *circa* 22 dB. Note this is for pyramidal absorber. An alternative choice would be to use, for example, wedge absorber along the side-walls. Although this approach reduces backscatter, it generally increases forward scatter which does not typically help in antenna pattern measurement applications [8]. Furthermore, the approximately rectangular cross-section of the reflector can be seen in the field illumination which clearly shows the cardinal form of the reflected field that will have greatest impact in the CATR antenna pattern measurements within the horizontal and vertical cuts [4, 8].

This form of simulation can also be used to determine the effect that the different feeds have on the chamber illuminations with broader feed pattern increasing the field

intensities around the BRE reflector. Thus, we can broadly conclude that the CATR serrated edges are to rolled edges as Chebyshev filters are to Butterworth filters, *i.e.* more pass-band ripple but with a faster roll off.

It is not just the illumination of the chamber walls that is of interest here, but also the amount of field that is reflected back towards the CATR feed. To illustrate this, the field reflected by the CATR reflector was computed over the surface of a plane that is transverse to the *z*-axis of the range and that intersects with the focal point. Fig. 8 presents false-color chalkboard plots of the electric field across this plane for the floor-fed serrated edge CATR, *cf.* Fig. 6a, a floor-fed blended rolled edge CATR, *cf.* Fig 6b and a corner-fed blended rolled edge CATR. Here, the feed tilt-angle was held fixed with the location of the feed being rotated by 45°. In practice, as a consequence of the geometry, it would be possible to increase the tilt angle within the confines of the chamber to move the feed into a region of lower field intensity. However, that improvement would be sought at the cost of increasing the cross-polar in the QZ. In each of these cases, the location of the feed, *i.e.* the position of the focal-point can be seen depicted by a white cross and aligns with, and is suggested by, the simulations presented in Fig. 7. It is clear that less field is reflected back to the feed for the serrated edge CATR than is the case for either of the blended rolled edge CATRs. The blended rolled edge reflector provides roughly equivalent reflected fields for the case of the floor-fed and corner-fed feeds as although the location of the feed has changed, the edges of the reflector have remained the same with respect to the chamber. This means that in addition to allowing the feed to be further displaced from the CATR QZ, by virtue of Pythagoras, the corner fed case means that less field is incident on, and therefore diffracted off, any feed baffle that is used to protect the QZ from direct illumination from the back-lobes of the CATR feed. Additionally, for the corner-fed case, the field drops-off more rapidly with distance so that increasing the feed tilt angle can provide a larger reduction in the amount of reflected field and VSWR that is a result of this. The serrated edge CATR case behaves very differently. Once the feed is positioned outside of the region of the pseudo-plane-wave, the field is relatively small and poorly controlled. As such, it varies in a far less well defined form.

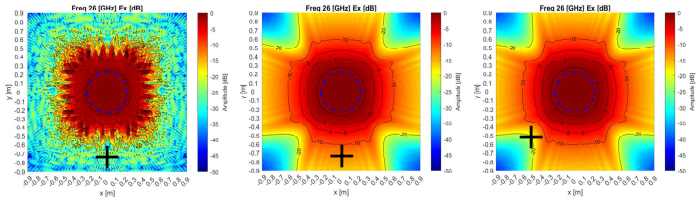

(a) (b) (c)

Fig. 8. Fields in focal plane for floor fed serrated edge CATR, (a) floor fed blended rolled edge CATR (b), corner fed blended rolled edge CATR (c) at 26 GHz.

As a final comment on the simulations presented in this section, it is perhaps useful to note how a three-dimensional oblong surface can be expressed conveniently in a polar form consisting of two independent variables. Thus, when computing the fields across the interior surface of the enclosing anechoic chamber, the Cartesian position coordinates were expressed as functions of two angles, *i.e.* the polar spherical angles θ, ϕ. When written in this form, the coordinates of the surface of a cuboid can be expressed as [11],

$$x = \frac{a\cos\theta\cos\phi}{2\sqrt{l}} \tag{1}$$

$$y = \frac{b\cos\theta\sin\phi}{2\sqrt{m}} \tag{2}$$

$$z = \frac{c\sin\theta}{2\sqrt{n}} \tag{3}$$

$$r = \sqrt{x^2 + y^2 + z^2} \tag{4}$$

Where,

$$l = 1 - s\left(\cos^2\theta\sin^2\phi - \sin^2\theta\right) \tag{5}$$

$$m = 1 - s\left(\cos^2\theta\cos^2\phi - \sin^2\theta\right) \tag{6}$$

$$n = 1 - s\cos^2\theta \tag{7}$$

Here, a is the x-axis width, b is the y-axis width, c is the z-axis width, and θ, ϕ are the spherical angles such that $-180° \le \theta \le 180°$, $0° \le \phi \le 180°$ where $0 \le s \le 1$. The parameter s has the effect that when $s = 0$, the shape is a sphere with radius r, when $s = 1$ the shape is a cube with edge length $2r$, and in between it is a three dimensional intermediate shape between the ellipsoid and the cuboid, *i.e.* a three-dimensional analogue of the two-dimensional squircle [11].

In practice then, the benefit in the CATR QZ of the BRE reflector is usually not so great as illustrated by typical physical-optics or geometrical-optics based QZ simulations as the redirected energy of the blended rolled edge needs to be effectively absorbed by the anechoic chamber walls for the full benefit to be achieved [8]. A consequence of the electrical size of the problem is that the task of predicting CATR QZ performance including the effects of the chamber remains a demanding task. However, as we have clearly demonstrated, wall illumination is a significant factor in the performance of a realized BRE CATR. Consideration of these effects within the design process is thus considered within the next section.

IV. Extended Broadband Genetic Optimisation for Chamber Effect Control and Minimisation

As illustrated within the previous section, wall illumination can be expected to be a far more significant contributor to the overall realized performance of a blended rolled edge CATR than is perhaps the case for a serrated edge CATR. For each elementary field component incident on the chamber walls, the reflected fields can be computed by, for example, resolving the incident fields onto parallel and perpendicular unit vectors and by using the TE (perpendicular) and TM (parallel) scattering matrix coefficients to compute the reflected elemental fields using [12],

$$\underline{E}_{reflec} = S_{11TE}\left(\underline{E}_i \cdot \hat{\underline{e}}_{TE}\right)\hat{\underline{e}}_{TE} + S_{11TM}\left(\underline{E}_i \cdot \hat{\underline{e}}_{TM}\right)\hat{\underline{e}}_{TM} \tag{8}$$

The total reflected field is obtained by integrating across all the elemental illuminating fields [12]. Here, S_{11TE}, S_{11TM} are the scattering matrix elements of the absorber which can be obtained either by simulation or measurement. These reflected fields can then be propagated to the CATR QZ using the same current elements based field propagation technique as is used for the CATR QZ simulation itself [4, 8]. The total field in the

QZ is the linear superposition of the feed spill-over, the direct illumination from the CATR reflector, and the fields reflected by the chamber walls. However, typically the effect of the fields when reflected by the absorber lining of the chamber are omitted from the CATR QZ performance predictions, as a consequence of the computational effort required and the accompanying typically long run-times.

Clearly, it would be advantageous if the genetic optimization could be extended to incorporate some consideration of these fields within the evolutionary process. That is to say, although computing the contribution of the scattered fields in the CATR QZ is a demanding task, and is presently beyond the ability of current desktop computing hardware to be able to incorporate it within the optimization loop of an evolutionary algorithm, calculating the field incident on the chamber walls and attempting to minimize it *is* tractable. For example, as the wall illumination can be seen to be relatively uniform and well behaved along the length of the side walls and ceiling of the chamber, *cf.* Fig 7b, it is sufficient to compute the field illuminating the walls in the specular region, *i.e.* half way between the QZ and the reflector in the cardinal points. In this way, it is possible to add these additional positions to those points in the QZ that are computed within the optimization loop. These fields may be treated separately by the penalty function, and this can be used to steer the evolutionary process. Adopting this strategy, the genetic optimizer was modified such that the algorithm attempted to minimize the chamber wall illumination while maximizing the uniformity of the pseudo plane-wave within the QZ. The algorithm was also modified to include the ability to place greater or lesser emphasis on minimizing the wall illumination so that QZ performance could be traded off against wall illumination. Fig. 9a contains the results of an initial optimization where a modest reduction in chamber illumination was sought while still attempting to preserve as much QZ performance as was possible. By comparing Fig 9a with Fig. 7b we can see that there has been a noticeable reduction in wall illumination. By way of a further test, Fig. 9b presents results where minimization of the wall illumination was further prioritized. Here, we can clearly see the wall illumination has been significantly reduced with the general fields far more closely resembling the fields produced by a serrated edge CATR, *cf.* Fig. 7a, with the wall illumination approaching a level of -20 dB along the centerline of the chamber walls.

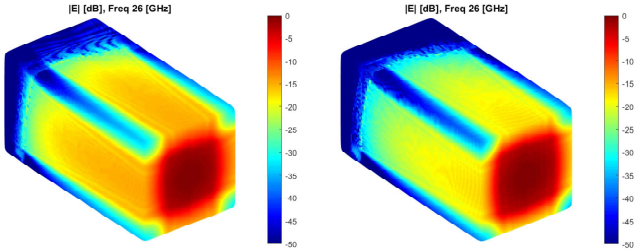

(a) (b)

Fig. 9. Comparison of CATR fields reflected from BRE reflector with wall constraint (a) and with strong wall constraint (b) at 26 GHz.

Clearly, there are limits as to what can be achieved here since we are merely varying the curvature of the edge of the BRE reflector, *cf.* Fig. 10 a, b, c, so that as we direct energy away from one direction (*i.e.* the chamber walls) we redirect it in another direction, which in this case is the CATR QZ where, crucially, we find the best absorber orientated optimally at normal incidence.

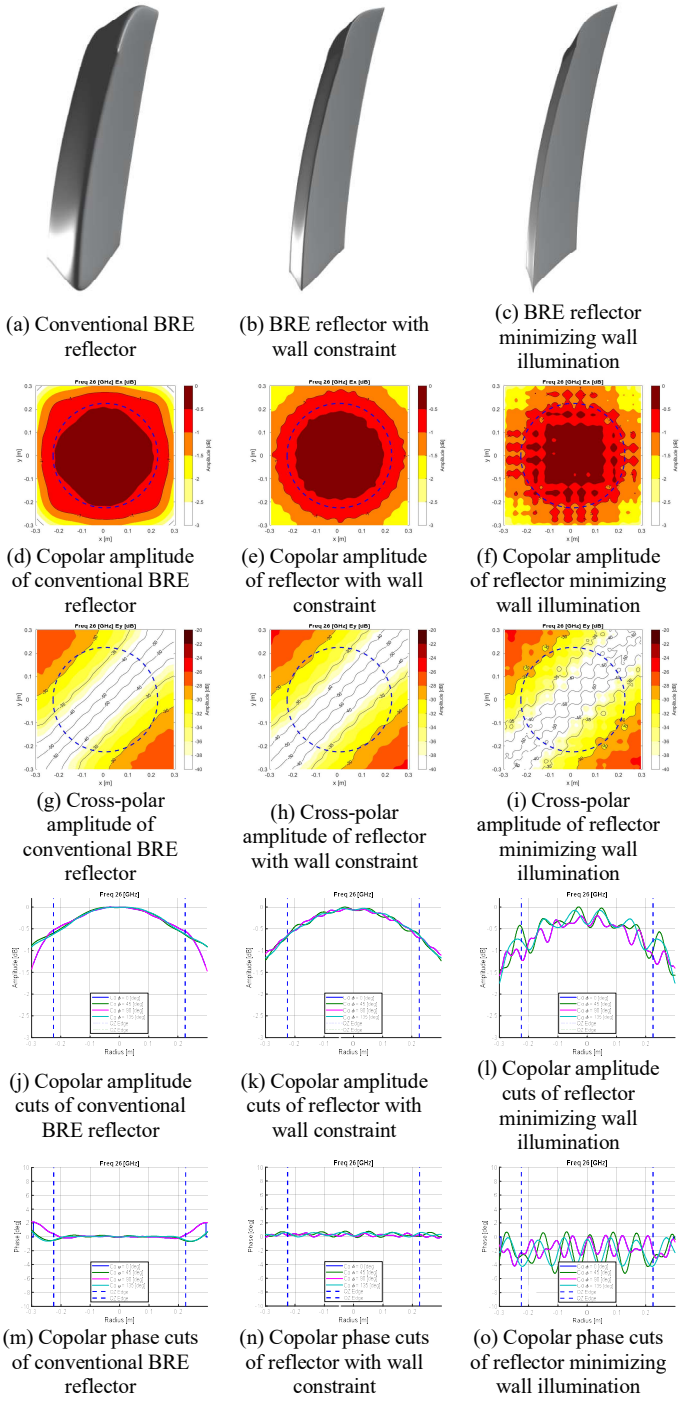

(a) Conventional BRE reflector
(b) BRE reflector with wall constraint
(c) BRE reflector minimizing wall illumination
(d) Copolar amplitude of conventional BRE reflector
(e) Copolar amplitude of reflector with wall constraint
(f) Copolar amplitude of reflector minimizing wall illumination
(g) Cross-polar amplitude of conventional BRE reflector
(h) Cross-polar amplitude of reflector with wall constraint
(i) Cross-polar amplitude of reflector minimizing wall illumination
(j) Copolar amplitude cuts of conventional BRE reflector
(k) Copolar amplitude cuts of reflector with wall constraint
(l) Copolar amplitude cuts of reflector minimizing wall illumination
(m) Copolar phase cuts of conventional BRE reflector
(n) Copolar phase cuts of reflector with wall constraint
(o) Copolar phase cuts of reflector minimizing wall illumination

Fig. 10. BRE CATR QZ predicted performance with a range of chamber wall illuminations at 26 GHz

Thus, as we direct more fields into the QZ we can expect to see some degradation in the QZ performance. The mechanism by which this has been achieved is changing the curvature of the BRE reflector. Where, the reduction in wall illumination

results from the smaller radius of curvature, *cf*. Fig. 10 a–c. It is therefore important to note that the reduction in the wall illumination has *not* been brought by means of a cancellation type effect. This geometrical change can therefore be expected to offer fairly broadband performance, and, although not shown as a consequence of limited space, this has been confirmed through further simulation.

Fig. 10 d–o present comparisons of the principal and cross-polarized amplitude and phase patterns as false color checkerboard plots and 0° (horizontal), 45° (inter-cardinal) and 90° (vertical) cuts for the three optimization cases considered above, *cf*. Figs 7b, 9a, and 9b. For the case where we attempt to minimize the wall illumination by 5 dB, *cf*. Fig 9b, we see that there is a marked increase in the QZ amplitude and phase ripple. When we back-off this requirement, *cf*. Fig 9a, we see that we are able to significantly reduce the degree of wall illumination whilst only minimally degrading the QZ performances, relative to the case where we optimize purely for QZ performance, *cf*. Fig 7b. In practice however, and as expounded above, the QZ performance will be impacted by the field that is scattered by the chamber and the ideal performance predicted in the left most column of Fig. 10 will not be fully achieved. However, and rather crucially, for the cases where the wall illumination has been reduced, this scattering contribution in the QZ will *also* be reduced. A summary of the QZ performance metrics can be seen presented in Table I that illustrates for all cases the CATRs comply with the standard 1 dB amplitude taper, 1 dB amplitude peak-to-peak ripple, and 10 deg peak-to-peak phase ripple specification [8]. Crucially, it can be seen that the reduced wall illumination case offers very nearly the same performance as the standard optimization cases with the benefit of the reduced chamber wall illumination.

TABLE I. CATR QZ PREDICTED PERFORMANCE AT 26 GHZ.

Parameter	Cut Angle ϕ [deg]	Standard Optimization	Reduced Wall Illumination	Minimized Wall Illumination
Amp Taper [dB]	0	0.59	0.65	0.75
	45	0.69	0.65	0.83
	90	0.59	0.65	0.75
Amp Ripple [dB]	0	0.08	0.08	0.48
	45	0.08	0.14	0.79
	90	0.08	0.08	0.48
Phase Ripple [deg]	0	0.65	0.58	3.32
	45	0.82	0.90	5.96
	90	0.68	0.58	3.32

V. SUMMARY AND CONCLUSION

In this paper we have verified the broadband performance of CATRs that were optimised at a variety of optimisation frequencies. The initial optimization at 40 GHz shows a very different result from the other frequencies and the re-optimization. This indicates a local minimum was found for which the mutation rate was not strong enough to escape. However, the refinement of the exit criteria has significantly reduced the sensitivity of the design to the specific optimisation frequency. The resulting reflector shapes now exhibit very stable shape characteristics over frequency, except at the lowest optimization frequency which is limited by the comparatively small electrical size of the reflector. The refined CATR geometrical characteristics have now been successfully deployed for 5G NR testing applications [10]. This paper also illustrated the difference in chamber wall illumination between serrated edge and blended rolled edge reflectors highlighting the latter's increased wall illumination, and the very notable benefits of the corner fed configuration. A revised optimisation strategy was then proposed which enabled a broadband reduction in chamber wall illumination to be achieved of ~5 dB for a BRE reflector by means of an adaptation to the curvature of the reflector. This was verified by simulation and was found to be realised across a broad range of frequencies. Lastly, as this is part of an ongoing study, the future work is to include obtaining further verification and considering more complex reflector edge treatments, further investigation of the broadband effects of the refined reflector design based on wall illumination reduction as well as optimised absorber treatment.

ACKNOWLEDGEMENT

The authors gratefully acknowledge the very valuable comments, corrections and suggestions of Prof. C.G. Parini.

REFERENCES

[1] M. Gustafsson, T. Jämsä, M. Högberg, "OTA Methods for 5G BTS Testing – Survey of Potential Approaches", 32nd URSI GASS, Montreal, 19-26 August 2017.

[2] 3GPP, "TR 37.842 v13.2.0 TSG RAN E-UTRA and UTRA; Radio Frequency (RF) requirement background for Active Antenna System (AAS) Base Station (BS)," 2017.

[3] C.G. Parini, S.F. Gregson, J. McCormick, D. Janse van Rensburg "Theory and Practice of Modern Antenna Range Measurements", IET Press, 2014, ISBN 978-1-84919-560-7.

[4] C.G. Parini, R. Dubrovka, S.F. Gregson, "Computational Electromagnetic Modeling of Compact Antenna Test Range Quiet Zone Probing: A Comparison of Simulation Techniques", EuCAP, Davos, 2016.

[5] S.F. Gregson, C.G. Parini, "Examination of the Effect of Common CATR Quiet Zone Specifications on Antenna Pattern Measurement Uncertainties", Loughborough Conference on Antennas and Propagation, Loughborough, November 2017.

[6] M. Dirix, S.F. Gregson, "Optimisation of the Serration Outline Shape of a Single Offset-Fed Compact Antenna Test Range Reflector Using A Genetic Evolution of the Superformula", EuCAP virtual conference, March 22-26 2021.

[7] M. Dirix, S. Gregson and R. Dubrovka, "Genetic Evolution of the Reflector Edge Treatment of a Single Offset-Fed Compact Antenna Test Range for 5G New Radio Applications," in AMTA Annual Meeting and Symposium, Daytona Beach, Florida, 2021.

[8] C.G. Parini, S.F. Gregson, J. McCormick, D. Janse van Rensburg, T. Eibert "Theory and Practice of Modern Antenna Range Measurements, 2nd Expanded Edition", IET Press, 2021, ISBN 978-1-83953-126.

[9] M. Dirix, S.F. Gregson, R. Dubrovka, "Genetic Evolution of the Reflector Edge Treatment of a Single Offset-Fed Compact Antenna Test Range for 5G New Radio Applications", AMTA 2021, October, Daytona, Florida, USA.

[10] S.F. Gregson, M. Dirix, R. Dubrovka, "Efficient Optimization of the Blended Rolled Edge of a Rectangular Single Offset-Fed Compact Antenna Test Range Reflector Using Genetic Evolution", EuCAP 2022, 27th March - 1st April, Madrid, Spain.

[11] C. Fong, "Analytical Methods for Squaring the Disc", International Congress of Mathematicians, ICM, Seoul, Korea, August, 2014.

[12] C.D. Finlay, S.F. Gregson, R.W. Lyon, J. McCormick, "SPIKE a Physical Optics based Code for the Analysis of Antenna Radome Interactions", RADAR 2007, Edinburgh International Conference Centre, Edinburgh, October 2007.